Thermal and optical characterization of resonant coupling between surface plasmon polariton and semiconductor waveguides

Joseph A. Summers and Rajeev J. Ram

Re-register for Table of Content Alerts

Create a profile. Sign up today!

Thermal and optical characterization of resonant coupling between surface plasmon polariton and semiconductor waveguides

Joseph A. Summers[a)] and Rajeev J. Ram
Research Laboratory of Electronics, Massachusetts Institute of Technology, Cambridge, Massachusetts 02139, USA

Resonant coupling between an Au-InP surface plasmon polariton (SPP) and an InP/InGaAsP ridge waveguide is investigated. The general design requirements for evanescent coupling between a low-loss waveguide and a highly absorptive SPP are described, and experimental results are presented for fabricated devices. Coupling from the ridge to the SPP is confirmed using fiber-to-fiber optical power measurements, and thermoreflectance imaging is used to directly measure power coupled to the SPP along the length of the metal waveguide. The role of the thin native oxide at the Au-InP interface is also explored and found to have a significant impact on coupling. © 2011 American Institute of Physics. [doi:10.1063/1.3658733]

The high optical mode confinement offered by surface plasmon polaritons (SPPs) has made SPP-based waveguides a promising area of research for realizing compact photonic devices, including polarizers, chemical sensors, and optical isolators.[1–7] Because SPP modes are guided at the interface between an intrinsically absorptive metal layer and a dielectric or semiconductor substrate, compact SPP mode size comes at the expense of greater propagation loss as the electric field overlaps more strongly with the metal. Absorption loss is especially severe on high-index semiconductor substrates, such as Si or InP, where the SPP mode confinement is higher than on dielectric substrates, and propagation loss is typically greater than $-0.5 \, \mathrm{dB}/\mu\mathrm{m}$ at telecommunications wavelengths ($\lambda = 1.55 \, \mu\mathrm{m}$).[8] This combination of high mode confinement and large propagation loss in SPPs makes it challenging to integrate them with existing semiconductor waveguide devices, such as lasers, modulators, and detectors. Though edge-coupling and evanescent coupling to SPPs have been demonstrated for low-confinement SPPs on dielectric substrates,[9,10] edge-coupling from semiconductor waveguides is inefficient due to the small SPP mode shape, while large propagation loss places tighter restrictions on evanescent coupling.

In this work, we present a hybrid semiconductor SPP waveguide design in which light is evanescently coupled between an InP/InGaAsP ridge waveguide and a highly absorptive Au-InP SPP. Experimental results are presented for fabricated devices, and resonant coupling between the ridge and SPP modes is independently verified using fiber-to-fiber optical power measurements and high-resolution thermal imaging of power absorbed by the SPP.

A schematic of the hybrid InP-SPP waveguide design is shown in Fig. 1(a). The design consists of an InP ridge waveguide topped with a layer of Au, where the thickness of the Au layer (>60 nm) has been chosen such that there is no interaction with the Au-air SPP mode at the top Au surface, and only the SPP mode at the Au-InP interface can couple to light in the semiconductor ridge. Since SPPs only support

TM polarization, the same basic co-directional coupler structure can be used as a waveguide polarizer by removing TM polarized light from the InP ridge. Such SPP-based polarizer designs have been described in earlier work using dielectric waveguides,[5–7] including the conditions that must be met for full resonant coupling from the semiconductor or dielectric waveguide to the SPP.[7] For lossy waveguides, a critical coupling condition must be satisfied that requires that the imaginary propagation constants of the supermodes be equal,

$$|A_2|e^{-\mathrm{Im}(\beta_2)L_C} = |A_1|e^{-\mathrm{Im}(\beta_1)L_C}. \tag{1}$$

Here, A_1 and A_2 represent the field amplitudes of the symmetric and antisymmetric supermodes of the coupled waveguides, β_1 and β_2 are their respective propagation constants, and L_C is the coupling length between the semiconductor waveguide and the SPP. It is assumed that for large separation of the waveguides, $Re(|\beta_1 - \beta_2|)$ approaches zero such that the two waveguides are phase-matched. For the case of a low-loss semiconductor waveguide coupled to a high-loss SPP, matching the imaginary propagation constants requires that the coupling length be on the same order as the attenuation length of the SPP, as observed in Ref. 11. The coupling length can be tailored to meet the critical coupling condition by choosing an appropriate InP upper cladding thickness, t. Finite element mode calculations of the supermodes' propagation constants as a function of upper cladding thickness are shown in Fig. 1(b), using the optical constants found in Refs. 12 and 13 at $\lambda = 1550 \, \mathrm{nm}$. The ridge and SPP modes are critically coupled, $Im(\beta_1) = Im(\beta_2)$, at an upper cladding thickness of 280 nm, for which the coupling length [$L_C = \pi/Re (|\beta_1 - \beta_2|) = 7 \, \mu\mathrm{m}$] is approximately equal to the supermodes' 3 dB attenuation length. This result is confirmed by eigenmode expansion (EME) simulations[14] of optical power in the ridge mode as a function of propagation length, shown in Fig. 1(c).

In order to test resonant coupling between the InP ridge and the Au-InP SPP, 1 mm-long ridge waveguides were fabricated with different metallization lengths, L_M. The semiconductor waveguide layer stack was epitaxially grown using metallorganic chemical vapor deposition on a

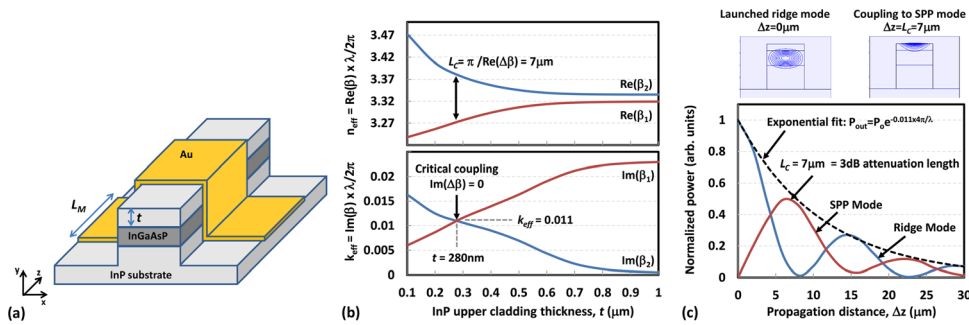a)Author to whom correspondence should be addressed. Electronic mail: summersjoseph@hotmail.com.

FIG. 1. (Color online) (a) Schematic of InP ridge-to-SPP coupler, illustrating metallization length, L_M, and InP upper cladding thickness, t. (b) Finite element calculations of the Au-metallized ridge TM supermodes as a function of t, showing (bottom) the critical coupling thickness, $t = 280$ nm, at which the imaginary effective supermode indices, k_{eff}, are equal, and (top) the real effective indices, n_{eff}, and the coupling length at the critical coupling thickness, $L_C = 7$ μm. (c) EME simulations of power in the metallized ridge for $t = 280$ nm, showing (top) the field intensity distribution, E_y^2, of the launched TM ridge mode and coupling to the SPP mode at the coupling length, and (bottom) power in the ridge and SPP modes as a function of propagation distance, where coupling length is equal to the 3 dB attenuation length.

Fe-doped InP substrate to provide the designed 610 nm-thick InGaAsP core ($\lambda_{bandgap} = 1.44$ μm) and 282 nm-thick InP upper cladding. Ridge waveguides were then patterned using photolithography and etched using reactive ion etching with methane/hydrogen/argon. Next, metallization regions were patterned on top of the ridge, and either Au or Fe/Au was deposited using DC magnetron sputtering. Finally, the substrate was lapped and facets were cleaved to allow fiber edge-coupling to the InP ridge waveguides.

The devices were characterized using two techniques: fiber-to-fiber optical power measurements to determine the optical power in the ridge waveguide and high resolution thermal imaging of the metallized ridge to measure optical power in the SPP mode. For fiber-to-fiber measurements, the input light was provided by an erbium doped fiber amplifier (EDFA) ($\lambda_{peak} = 1550$ nm) that was polarized using an inline fiber polarizer, and edge-coupled to the TM mode of the waveguides using a polarization maintaining (PM) lensed fiber mounted on a fiber rotation chuck. The output facet was then edge-coupled to a single-mode lensed fiber and connected to a photodetector to measure optical power. Both the input and output fibers were mounted on piezo-controlled flexure stages to enable fine control of coupling.

Thermal imaging of the SPP was done with lock-in thermoreflectance (TR) thermography using a charged-coupled device (CCD) camera for a detector[15–17] TR measures the relative change in surface reflectivity ($\Delta R/R$) caused by a change in temperature (ΔT), as described by the relationship $\Delta R/R = \kappa \Delta T$. The TR coefficient, κ, is typically very small (10^{-5}–10^{-3} K^{-1}), therefore a "four-bucket" lock-in technique is used to improve sensitivity.[16,17] Since the spatial resolution of the thermal image is determined by the optical resolution of the imaging system, submicron spatial resolutions are easily attainable using high numerical aperture (NA) objectives and illumination wavelengths in the visible spectrum.[17] For the SPP thermal measurements, the entire surface of a 30 μm-long Au-metallized ridge was imaged onto a 640 × 480 pixel CCD camera using a microscope with a 100×, 0.7 NA objective and a blue LED for illumination ($\lambda_{peak} = 470$ nm). The same experimental setup was previously used to calibrate $\kappa = 3.3 \times 10^{-4}$ K^{-1} for Au with blue LED illumination,[16] and the Rayleigh criterion gives a thermal spatial resolution of 410 nm. In order to increase the

absorbed power and temperature swing in the SPP, a distributed feedback (DFB) laser was used as the light source ($\lambda_{DFB} = 1544$ nm) and placed before the EDFA to provide $\sim$1 mW into the device after taking into account $\sim$10 dB of fiber-to-facet coupling loss. The DFB laser current was modulated at a frequency $f_{mod} = 15$ Hz and phase locked to the CCD camera which captured four microscope images of the device per modulation period at 60 fps. The device images were then post-processed in the computer to calculate the relative change in reflectivity per pixel ($\Delta R/R$), yielding a temperature map of the device and showing regions where the pump laser was strongly absorbed by the metal.

Measurement results for the Au-metallized chips are shown in Fig. 2. Fiber-to-fiber optical power measurements are shown at the bottom and compared to EME simulations of power in the ridge waveguide as a function of metallization length, L_M. Power measurements were taken on two chips, each with 14-15 rows of metallized waveguides, with L_M ranging from 0 to 29.8 μm, and ridge width measured to be
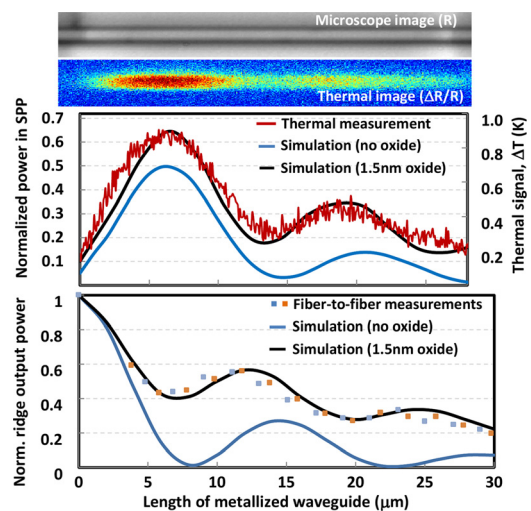

FIG. 2. (Color online) (top) Microscope and TR images of the Au-metallized InP ridge waveguide, showing the temperature rise due to optical power absorbed by the SPP, (center) temperature profile along the length of the metallized ridge, compared to EME simulations of power in the SPP. Including a 1.5 nm-thick native oxide at the Au-InP interface in the simulation provides good agreement with measurements, (bottom) fiber-to-fiber optical power measurements compared to simulations of optical power in the ridge.
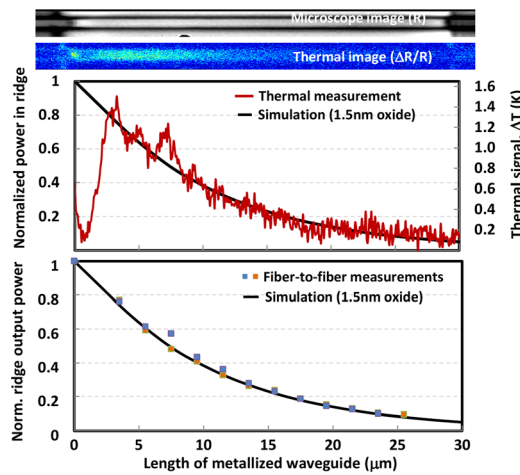
FIG. 3. (Color online) (top) Microscope and thermoreflectance images of the Fe-metallized InP ridge waveguide, showing the temperature rise due to optical power absorbed by the Fe, (center) temperature profile along the length of the metallized ridge, compared to EME simulations of power in the ridge, (bottom) fiber-to-fiber optical power measurements compared to simulations of optical power in the ridge. Metallized waveguide loss for both measurements ($\alpha = 970$/cm) are in good agreement with simulation ($\alpha = 1010$/cm).

1.4 μm using a scanning electron microscope (SEM). Dips in output power can be seen at metallization lengths of 8 μm and 20 μm, indicating resonant coupling to the SPP ($L_M = L_C$). Good agreement between the simulation and measurements can be obtained by including a native oxide layer between the InP surface and the Au layer in the model. Assuming a native oxide refractive index of n = 1.5 (Ref. 18) and by using oxide thickness as a fitting parameter, the best agreement can be found for an oxide thickness of 1.5 nm, which is similar to reported thicknesses for native oxides on InP.[19]

Thermoreflectance measurements are shown at the top of Fig. 2 and plotted alongside EME simulations of power in the SPP mode. Local maxima in temperature can be seen at a propagation distances of 7 μm and 19 μm, in good agreement with the 12 μm beat length seen in the fiber-to-fiber measurements, and indicating strong absorption in the metal and coupling to the SPP. As with the fiber-to-fiber simulations, the best agreement with thermal measurements was found by including in the model a 1.5 nm-thick native oxide at the Au-InP interface.

In order to compare the Au-InP SPP results to a more absorptive, non-resonantly coupled metal, Fe-clad InP ridge waveguides were also fabricated. A 100 nm-thick layer of Fe was deposited and capped with a 50 nm-thick layer of Au to prevent oxidation and enhance thermal imaging. Fiber-to-fiber measurements were taken on two chips, each with 15 rows of metallized waveguides with L_M ranging from 0 to 25.5 μm, and a ridge width of 1.2 μm (Fig. 3, bottom). Fitting an exponential to the fiber-to-fiber measurements [$P(z) = P_o e^{-\alpha z}$] gives a measured $\alpha = 970$/cm, which is in excellent agreement with the simulated loss ($\alpha = 1010$/cm), using the optical constants for Fe provided in Ref. 20.

Thermoreflectance measurements are shown at the top of Fig. 3 and compared to simulations of power in the absorptive ridge mode. A large dip in the thermal signal can be seen for the first couple of microns of propagation in the metallized waveguide and is due to heat spreading from the thick buildup of metal at the photoresist sidewall during sputtering. Ignoring the dip, however, and fitting an exponential to the thermoreflectance measurements gives a measured $\alpha = 970$/cm, which matches the fiber-to-fiber measurements and is also in excellent agreement with simulations ($\alpha = 1010$/cm).

In summary, we have demonstrated resonant coupling between an InP ridge waveguide and an absorptive Au-InP SPP. Thermal imaging of the SPP and fiber-to-fiber optical measurements were used to independently verify coupling to the SPP, and two different metals (Au and Fe) were deposited and measured to compare resonant versus non-resonant coupling. Good agreement between simulation and measurement was obtained by including a 1.5 nm-thick native oxide in the model at the Au-InP interface, which was shown to have a significant impact on coupling.

[1]W. L. Barnes, A. Dereux, and T. W. Ebbesen, Nature **424**, 824 (2003).
[2]S. A. Maier and H. A. Atwater, J. Appl. Phys. **98**, 011101 (2005).
[3]J. Montoya, K. Parameswaran, J. Hensley, M. Allen, and R. Ram, J. Appl. Phys. **106**, 023108 (2009).
[4]J. B. Khurgin, Appl. Phys. Lett. **89**, 251115 (2006).
[5]W. Johnstone, G. Stewart, T. Hart, and B. Culshaw, J. Lightw. Technol. **8**, 538 (1990).
[6]T. Nakano, K. Baba, and M. Miyagi, J. Opt. Soc. Am. **11**, 2030 (1994).
[7]C.-H. Chen and L. Wang, IEEE J. Quantum Electron. **34**, 1089 (1998).
[8]C. G. Durfee, T. E. Furtak, R. T. Collins, and R. E. Hollingsworth, J. Appl. Phys. **103**, 113106 (2008).
[9]T. Nikolajsen, K. Leosson, I. Salakhutdinov, and S. I. Bozhevolnyi, Appl. Phys. Lett. **82**, 668 (2003).
[10]R. Wan, F. Liu, Y. Huang, S. Hu, B. Fan, Y. Miura, D. Ohnishi, Y. Li, H. Li, and Y. Xia, Appl. Phys. Lett. **97**, 141105 (2010).
[11]Y.-C. Lu, W.-P. Huang, and S.-S. Jian, J. Lightw. Technol. **27**, 4804 (2009).
[12]J. P. Weber, IEEE J. Quantum Electron. **30**, 1801 (1994).
[13]E. D. Palik, *Handbook of Optical Constants of Solids* (Academic, New York, 1985).
[14]FimmWave/FimmProp v5.2 by Photon Design Ltd., Oxford, UK.
[15]M. Farzaneh, K. Maize, D. Luerrsen, J. A. Summers, P. M. Mayer, P. E. Raad, K. P. Pipe, A. Shakouri, R. J. Ram, and J. A. Hudgings, J. Phys. D: Appl. Phys. **42**, 143001 (2009).
[16]S. Grauby, B. C. Forget, S. Hole, and D. Fournier, Rev. Sci. Instrum. **70**(9), 3603 (1999).
[17]P. M. Mayer, D. Luerrsen, R. J. Ram, and J. A. Hudgings, J. Opt. Soc. Am. A **24**, 1156 (2007).
[18]H. J. Lewerenz, D. E. Aspnes, B. Miller, D. L. Malm, and A. Heller, J. Am. Chem. Soc. **104**(12), 3325 (1982).
[19]A. Guivarc'h, H. L'Haridon, G. Pelous, G. Hollinger, and P. Pertosa, J. Appl. Phys. **55**, 1139 (1984).
[20]M. A. Ordal, L. L. Long, R. J. Bell, S. E. Bell, R. R. Bell, R. W. Alexander, and C. A. Ward, Appl. Opt. **22**, 1099 (1983).